A&A, 694, A7 (2025)
https://doi.org/10.1051/0004-6361/202450951
© The Authors 2025

Astronomy & Astrophysics
Special issue

ZTF SN Ia DR2

ZTF SN Ia DR2: Exploring SN Ia properties in the vicinity of under-dense environments

M. Aubert[1,⋆], P. Rosnet[1], B. Popovic[2], F. Ruppin[2], M. Smith[3], M. Rigault[2], G. Dimitriadis[4], A. Goobar[5], J. Johansson[5], C. Barjou-Delayre[1], U. Burgaz[4], B. Carreres[6,7], F. Feinstein[6], D. Fouchez[6], L. Galbany[8,9], M. Ginolin[2], T. de Jaeger[10], M. M. Kasliwal[11], Y.-L. Kim[3], L. Lacroix[5,10], F. J. Masci[12], T. E. Müller-Bravo[8,9], B. Racine[6], C. Ravoux[1], N. Regnault[10], R. L. Riddle[13], D. Rosselli[6], B. Rusholme[12], R. Smith[13], J. Sollerman[14], J. H. Terwel[4,15], and A. Townsend[16]

[1] Université Clermont Auvergne, CNRS/IN2P3, LPCA, F-63000 Clermont-Ferrand, France
[2] Univ Lyon, Univ Claude Bernard Lyon 1, CNRS, IP2I Lyon/IN2P3, UMR 5822, F-69622 Villeurbanne, France
[3] Department of Physics, Lancaster University, Lancs LA1 4YB, UK
[4] School of Physics, Trinity College Dublin, College Green, Dublin 2, Ireland
[5] The Oskar Klein Centre, Department of Physics, Stockholm University, SE-10691 Stockholm, Sweden
[6] Aix Marseille Université, CNRS/IN2P3, CPPM, Marseille, France
[7] Department of Physics, Duke University, Durham, NC 27708, USA
[8] Institute of Space Sciences (ICE-CSIC), Campus UAB, Carrer de Can Magrans, s/n, E-08193 Barcelona, Spain
[9] Institut d'Estudis Espacials de Catalunya (IEEC), 08860 Castelldefels (Barcelona), Spain
[10] LPNHE, CNRS/IN2P3, Sorbonne Université, Université Paris-Cité, Laboratoire de Physique Nucléaire et de Hautes Énergies, 75005 Paris, France
[11] Division of Physics, Mathematics, and Astronomy, California Institute of Technology, Pasadena, CA 91125, USA
[12] IPAC, California Institute of Technology, 1200 E. California Blvd, Pasadena, CA 91125, USA
[13] Caltech Optical Observatories, California Institute of Technology, Pasadena, CA 91125, USA
[14] Department of Astronomy, The Oskar Klein Center, Stockholm University, AlbaNova 10691 Stockholm, Sweden
[15] Nordic Optical Telescope, Rambla José Ana Fernández Pérez 7, ES-38711 Breña Baja, Spain
[16] Institut für Physik, Humboldt-Universität zu Berlin, Newtonstr. 15, 12489 Berlin, Germany

Received 31 May 2024 / Accepted 3 September 2024

ABSTRACT

Context. The unprecedented statistics of detected Type Ia supernovae (SNe Ia) brought by the Zwicky Transient Facility (ZTF) enable us to probe the impact of the large-scale structure (LSS) on the properties of these objects.
Aims. The goal of this paper is to explore the possible impact of the under-dense part of the LSS on the intrinsic SALT2 light-curve properties of SNe Ia and uncover possible biases in SN Ia analyses.
Methods. With a volume-limited selection of ZTF-Cosmo-DR2 SNe Ia overlapping with the SDSS-DR7 survey footprint, we investigated the distribution of their properties with regard to voids detected in the SDSS-DR7 galaxy sample. We further used Voronoi volumes as a proxy for local density environments within the LSS.
Results. We find a moderate dependency of the stretch on the localisation around the void centre and none when considering colour. The local Voronoi volumes mostly affect the fraction of low- and high-stretch supernovae.
Conclusions. With the presently available statistics, we consider that the impact of high- or low-local-density environment can be considered as a proxy for the colour of the host galaxy. Under-dense environments should not cause any biases in analyses of supernova.

Key words. supernovae: general – cosmology: observations – large-scale structure of Universe

1. Introduction

Type Ia supernovae (SNe Ia) are commonly used as distance indicators in astronomy to map the Universe at cosmological scales. Due to the underlying physics phenomenon triggering such transient events, namely white-dwarf thermonuclear explosions (Hoyle & Fowler 1960), SNe Ia constitute standardisable candles. As such, they enabled the discovery of the accelerated expansion of the Universe in the late 90s (Riess et al. 1998; Perlmutter et al. 1999) and remain a key probe with which to constrain deviations from the standard model of cosmology through the estimation of the Hubble constant (Freedman 2021; Riess et al. 2022), or the dark energy equation of state (Brout et al. 2022; Abbott et al. 2024).

The luminosity distance of SN Ia is estimated using the empirical Tripp relation (Tripp 1998) based on the properties of their light curves: (i) the broader the light-curve shape, the brighter the SN Ia (Phillips 1993), and (ii) the redder the light curve, the fainter the SN Ia (Riess et al. 1996). The basic standardisation procedure corrects those two effects linearly in order

⋆ Corresponding author; marie.aubert@clermont.in2p3.fr

Open Access article, published by EDP Sciences, under the terms of the Creative Commons Attribution License (https://creativecommons.org/licenses/by/4.0), which permits unrestricted use, distribution, and reproduction in any medium, provided the original work is properly cited.
This article is published in open access under the Subscribe to Open model. Subscribe to A&A to support open access publication.

to decrease the intrinsic dispersion of the absolute magnitudes of SN Ia at maximum luminosity.

The current state of the art in SN Ia standardisation uses the SALT2 model (Guy et al. 2007, 2010), or its improved version SALT3 (Kenworthy et al. 2021), to determine the two parameters entering the Tripp relation: (i) the stretch, which is the broadening of the light curve, and (ii) the colour to account for its redness. Nevertheless, beyond the two-term correction, an environmental dependency was observed, first with the mass of the host galaxy; the two-term-corrected luminosity is brighter for SNe Ia in massive host galaxies (Kelly et al. 2010; Sullivan et al. 2010; Lampeitl et al. 2010). By adding the mass-step term as an environmental dependency in the standardisation procedure, the residual dispersion in the Hubble-Lemaître diagram is typically 0.12 mag (Brout et al. 2022; Popovic et al. 2024; Rubin et al. 2023; Abbott et al. 2024).

Since the initial discovery of the SN Ia brightness correlation with the stretch parameter, it has also been identified that the stretch parameter is connected to the host properties, such as the galaxy morphology (Filippenko 1989; Hamuy et al. 1996 and Pruzhinskaya et al. 2020 for a more recent study) or other environmental tracers (Sullivan et al. 2010; Rigault et al. 2020; Kim et al. 2018, 2019). As galaxy properties evolve over time, Childress et al. (2014) predicted that SN Ia properties could suffer changes over cosmic time. Nicolas et al. (2021) uncovered evidence for a redshift drift of the SN Ia stretch distribution, and Möller et al. (2024) also observed such a shift in the DES Y5 high-redshift sample. In addition to the correlation between the stretch and environment, it appears that the linear stretch–magnitude relation is broken, as shown in Ginolin et al. (2024), suggesting that the standardisation process of the stretch is itself dependent on both redshift and environment.

The colour of SNe Ia has also been found to be weakly correlated with the galaxy host environment (Childress et al. 2013; Popovic et al. 2021; Kelsey et al. 2023). In addition, evidence of this SN Ia parameter dependency with respect to redshift has recently emerged, as summarised in the ZTF-DR2-Cosmo companion paper (Popovic et al. 2025).

Beyond the host-galaxy properties, a new question arises pertaining to the possible correlation between SN Ia properties and the large-scale structure (LSS) of the Universe. Indeed, the LSS traced by matter shows a complex web of structures delineating filaments, walls, clusters, and cosmic voids, all with very specific properties. Supernovae in general have been confirmed to reproduce the clustering of matter in the Universe (Tsaprazi et al. 2022); however, the dependency of specific SN properties on these environments has not been extensively explored. While a first study found tentative evidence of a correlation between the stretch of SNe Ia and their proximity to galaxy clusters, the densest part of the large-scale structure (Xavier et al. 2013; Toy et al. 2023; Larison et al. 2024; Ruppin et al. 2025), other extreme density environments are found within the cosmic web: cosmic voids.

Cosmic voids are under-dense extended structures of the LSS within which less matter and fewer galaxies are observed on average. Since their discovery in the LSS (Gregory & Thompson 1978; Jôeveer et al. 1978) and thanks to the increased statistics provided by large redshift surveys, voids have been detected (Hoyle et al. 2005; Pan et al. 2012; Mao et al. 2017) and extensively studied in order to extract cosmological constraints using their size distribution (Sheth & van de Weygaert 2004; Pisani et al. 2015; Contarini et al. 2019, 2022), cross-correlation function with galaxies (Woodfinden et al. 2022; Aubert et al. 2022; Hamaus et al. 2022; Radinović et al. 2023), and lensing signal (Krause et al. 2013; Sánchez et al. 2017; Bonici et al. 2023); see Pisani et al. (2019) and references therein for a review.

The aim of the analysis presented in this paper is to study potential correlations between the properties of the light curves of SN Ia and the LSS of the Universe, focusing on its under-dense parts. Parts of our analysis are complementary to the results of Ruppin et al. (2025), who performed a similar analysis but dedicated to clusters. The analysis is based on the second data release of SNe Ia from the Zwicky Transient Facility (ZTF), here referred to as the ZTF-Cosmo-DR2 sample (Rigault et al. 2025). The paper is structured as follows: Section 2 describes the SN Ia and cosmic voids sample selection and creation for our analysis. Section 3 investigates SN Ia properties in the vicinity of voids. In Section 4, we present the repartition and properties of SNe Ia with regard to the local large-scale density provided by Voronoi volumes. Finally, we discuss our results in Section 5 and conclude in Section 6.

2. Data samples

We first describe the ZTF-Cosmo-DR2 sample. We then explain the creation process of the void catalogues at low redshift as well as the derived quantities used in this paper. Finally, we present the final samples used in the paper.

2.1. The ZTF SNe Ia sample COSMO-DR2

The particularity of the ZTF survey (Bellm et al. 2019; Graham et al. 2019) is that the visible sky (the northern sky above a declination of −30 deg) is scanned more than once per night thanks to the large field of view of its camera, which covers 47 deg^2 (Dekany et al. 2020). The analysis of the observations (Masci et al. 2019) ranging from 2018 to 2020, corresponding to the first stage of ZTF (ZTF-I), led to a unique data set – the ZTF-Cosmo-DR2 – of more than 3000 spectroscopically classified SNe Ia in the nearby Universe, with cosmological redshifts of $z \leq 0.15$ (Rigault et al. 2025). The SN Ia classification was based on spectrum acquisition using the Spectral Energy Distribution Machine (SEDm, Blagorodnova et al. 2018; Rigault et al. 2019; Kim et al. 2022) for the most part, with additional contributions discussed in Smith et al. (2025). SNe Ia were further classified into different subtypes, such as 'norm', 'pec-91bg', and 'pec-91t'; details concerning the classification of SNe Ia and further analysis are provided in Smith et al. (2025), Dimitriadis et al. (2025), Burgaz et al. (2025). From this sample, we obtain a volume-limited sample of almost 1200 SNe Ia up to $z < 0.06$ (Amenouche et al. 2025). The host galaxy redshift is available for 60% of the volume-limited sample, with the remainder of the SN Ia redshifts being estimated from the SN Ia spectra, representing an unprecedentedly well-characterised sample of SNe Ia.

The light curves of this data set were fitted with the help of the SALT2.4 model (Guy et al. 2007, 2010; Betoule et al. 2014), using Taylor et al. (2023) retraining to extract their stretch (x_1) and colour (c) parameters used for their standardisation (Smith et al. 2025). The aim of this analysis is not to compute the corrected distance modulus as a distance indicator for cosmological analysis, but to try to see if cross-correlations exist between the properties of the light curves of SN Ia (x_1 and c) and the LSS of the Universe, focusing on the properties of cosmic voids.

To this end, we only consider the volume-limited SNe Ia within the redshift range $z = [0.02, 0.06]$, which overlaps with

the LSS catalogue of galaxies and voids defined below. Further details of this selection are provided in Sect. 2.3.

2.2. SDSS DR7: Void and galaxy samples

In this subsection, we first present the source galaxy sample and the data selection used to identify cosmic voids. We then briefly describe the void identification process and the quality cuts applied to our catalogues.

In order to define the large-scale environment, we make use of the DR7.2 NYU value-added galaxy catalogues (NYU-VAGC)[1] (Blanton et al. 2005; Padmanabhan et al. 2008) built from the seventh data release of the Sloan Digital Sky Survey collaboration (SDSS-DR7) (Abazajian et al. 2009). In particular, we make use of the `full0` galaxy catalogue, which is dedicated to LSS studies. This catalogue includes all available objects in the spectroscopic footprint of the SDSS-DR7 survey. From this sample, we first select the contiguous footprint area of the north galactic cap of 6960 deg^2 with an 80% lower limit requirement for the completeness. The completeness indicates the number of galaxies whose redshift was measured out of the total number of sources observed in the photometric survey.

We then select all the available galaxies in the redshift range $z = [0.018, 0.11]$, yielding 341 433 objects. The selected redshift range largely encapsulates that of the first selection applied to the SNe Ia sample. The minimum redshift is defined so as to be wider than that of the SN Ia selection in order to mitigate possible boundary effects. Similarly, we deliberately set an arbitrarily high redshift as the upper boundary in order to remove any boundary effects in the vicinity of the most populated redshift range of the selected SN Ia sample.

To identify voids, we make use of the real-space void Locations from survey reconstruction (Revolver) algorithm (Nadathur et al. 2019), which is similar to the void identification and examination toolkit (VIDE) algorithm (Sutter et al. 2015), itself based on the underlying Zone Bordering on Voidness (ZOBOV) algorithm (Neyrinck 2008), which applies a Voronoi tessellation scheme to the galaxy comoving coordinates. The Voronoi tessellation paves the three-dimensional space occupied by a discrete distribution of points. A Voronoi cell is defined around each point (i.e. galaxy) by tracing all the bisectors between the considered point and its surrounding neighbours. Each Voronoi cell therefore encloses all the nearest neighbouring space to a point. The resulting volume of the cell V_c, shaped as a polyhedron, provides an estimation of the local density $\rho_{loc} = 1/V_c$ in the vicinity of the point.

The void-finding process goes through three stages. First, the Revolver algorithm converts the positions to comoving coordinates using a given Flat-ΛCDM fiducial cosmology. In the present paper, the adopted fiducial cosmology is set to $\Omega_m = 0.31$ hereafter, and all distances are quoted in Mpc h^{-1}.

The algorithm adds fake galaxy positions within the holes of the survey footprint and at its angular and redshift edges in order to bind the volume to which the Voronoi tessellation is applied, acting as a buffer to prevent strong edge effects. The angular footprint is provided by a Healpix map. The latter is generated from the `mangle` polygons describing the footprint of the SDSS-DR7 survey (Swanson et al. 2008; Hamilton & Tegmark 2004). The ZOBOV algorithm then implements the Voronoi tessellation, which is applied to all the tracers, including the generated buffer galaxies. In order to prevent natural growth of the volumes with redshift and to account for incompleteness in the survey, weight corrections are applied to the Voronoi volumes. The weights applied to these volumes depend on two quantities: the completeness (the volume will be decreased if the completeness is low), and the selection function, which will correct for eventual variations of the number density of objects as a function of redshift.

From the resulting corrected Voronoi volumes $V_{w,c}$, local density minima are identified in the tessellated space and are merged – through an iterative process – to their adjacent low-density cell, without applying any threshold using the principle of the Watershed method. The latter is akin to flooding low density regions (local density minima) with water until the water level of adjacent regions meets at the ridges separating these regions, therefore defining boundaries between regions.

This merging process creates zones of low-density Voronoi cells, which we define as voids in the input tracer sample. This process can be reiterated to merge zones into larger structures; however, the Revolver algorithm does not apply this merging further in order to define a void as the smallest under-dense entity. The voids identified with the Revolver tessellation-based algorithm are therefore large under-dense regions constructed with adjacent low-density Voronoi cells built around isolated galaxies in the input galaxy sample.

From the resulting information brought by both Voronoi tessellation and member galaxy positions, one can then extract the basic properties of the voids:

- The Voronoi volume V_c associated with each galaxy in the sample.
- The weighted Voronoi volume $V_{w,c}$ associated with each galaxy in the sample.
- The void radius: The void finder and subsequent void definition do not impart any shape to the detected voids. The void radius is therefore derived from the total volume of the N_g Voronoi cells defining the void reduced to that of a spherical radius quantity (1):

$$r_v = \left(\frac{3}{4\pi} \sum_i^{N_g} V_c^i \right)^{1/3}. \quad (1)$$

- Void centre: The Voronoi volume-weighted barycentre (2) of the member galaxies of the void:

$$\boldsymbol{X}_v = \frac{1}{\sum_i^{N_g} V_c^i} \sum_i^{N_g} V_c^i \boldsymbol{X}_g^i. \quad (2)$$

During the process of associating the Voronoi cells into voids – see Fig. 1 of Neyrinck (2008) for a 2D illustration – galaxies adjacent to the buffer particles are flagged and taken into account in the construction of the void structures. Voids close to or associated with these flagged galaxies are considered edge voids and are discarded in our final selection to obtain a conservative void catalogue. We apply a final conservative cut on the void radius of $r_v \geq 10$ Mpc h^{-1}, corresponding to a value approaching four times the mean particle separation (MPS), which is the average distance between galaxies in the sample and is about 2.5 Mpc h^{-1}. This allows us to select voids that should be exempt from strong non-linear effects. Figure 1 displays the void radius distribution, and the redshift distributions of both voids and galaxies. Our void sample contains 592 voids up to a redshift of $z < 0.11$, which reduces to 193 voids with redshifts below $z < 0.07$.

In addition to the void sample, we also possess information on the local density around each galaxy, which is provided

[1] http://sdss.physics.nyu.edu/vagc/lss.html

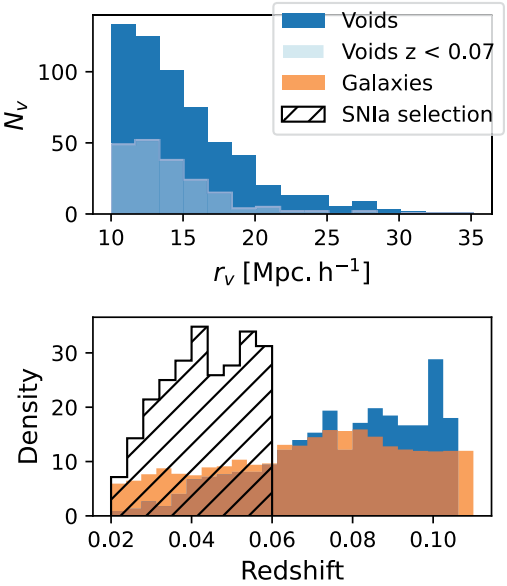

Fig. 1. Summary statistics distribution. The top panel shows the void radius distribution up to $z < 0.11$ in blue and the void radius distribution with $z < 0.07$ in lighter blue. The bottom panel shows the void, galaxy, and SN Ia redshift distributions.

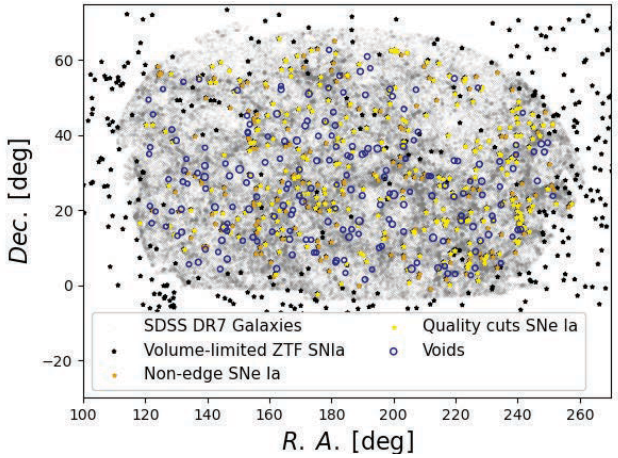

Fig. 2. Angular distributions of the volume-limited ZTF-Cosmo-DR2 (black stars), the reduced SN Ia sample after selection cuts (yellow stars), and voids (dark blue circles) superimposed on the SDSS DR7 galaxy selection (transparent grey markers). For the voids, the marker sizes scale with void radius.

Table 1. Summary of the numbers of each tracer.

Objects	In SDSS	Quality cuts
SNe Ia	448	281
	Total	z <0.07
Galaxies	341 433	157 083
Voids	592	193

Notes. For SNe Ia, we quote the number within the SDSS sample, both in the volume-limited prescription and after quality cuts. For galaxies, we quote the original selection and the $z < 0.07$ reduced count. For voids, we quote the final selection, including edge cuts and radius cuts, as 'Total' and the same sample with the added redshift cut $z < 0.07$.

by the weighted Voronoi volumes $V_{w,c}$. This local density estimation can be used as a marker of the isolation of galaxies to test the dependency of object properties (SNe Ia or galaxies) on the underlying local density field (Habouzit et al. 2020). It also enables us to complement the LSS classification, by avoiding potential systematic effects in the void-finding process. Such systematic errors, for example, might be the inclusion of high-density galaxies in the ridge of the void, as recently evidenced in the work of Zaidouni et al. (2024).

2.3. Matching SNe Ia and final data selection

For the purpose of our study, we first select all the SNe Ia falling within the observed high completeness footprint of the SDSS DR7 NYU-VAGC. From this selection, we then consider only the volume-limited sample of SNe Ia by restricting our sample to redshifts of $z < 0.06$.

All of these SNe are then matched to their nearest neighbouring galaxy and void. We use a space-partitioning data structure k-D Tree, which organises points into a k-dimensional space, which in our case is 3D space. This data structure enables us to quickly and efficiently find the nearest neighbours in the tree to a given point; we build trees with void and galaxy comoving coordinates using `scikit-learn`'s KDTree feature (Pedregosa et al. 2011). By querying these trees, we obtain the nearest neighbouring galaxy or void to each SNe Ia in the SDSS footprint. We also obtain the comoving separation distance between the SNe Ia and both nearest neighbouring objects. From this information, we discard all the SNe Ia in each sample whose nearest neighbouring galaxy is flagged as an edge galaxy.

The total number of SNe Ia enclosed within the galaxy sample is therefore 448. We further refined the SN Ia sample by applying similar quality cuts as detailed in Ginolin et al. (2024). The considered cuts are the following: good light-curve sample with at least seven 5σ level detections within the -10 to $+40$ days phase range considered, among which two pre- and post-max detections, respectively, and a detection in at least two of the ZTF bands (g, r, i), an absolute stretch parameter $|x_1| < 3$ with an error of $\sigma_{x_1} < 1$, a colour $c \in [-0.2, 0.8]$ with an error of less than $\sigma_c < 0.1$, an error on the estimated time of the peak luminosity of below 1 day, $\sigma_{t_0} < 1$ day, and finally, a SALT2 light-curve fit probability of greater than 10^{-7}. Considering the quality cuts, the total number of SNe Ia considered in this paper, unless stated otherwise, is 281. Figure 2 displays the SDSS-DR7 galaxies, superimposed with the angular positions of the original volume-limited SNe Ia sample, the reduced SNe Ia sample, and the void sample. SNe Ia within the footprint shown in black are SNe Ia discarded due to their direct proximity to edge galaxies. The considered counts for each tracer (SNe Ia, galaxies, and voids) are quoted in Table 1 and the resulting SN Ia redshift distribution is shown in the lower panel of Fig. 1. We note that no further selection is performed on the SN Ia sample; we therefore consider all SNe Ia regardless of their proximity to dense or under-dense environment.

3. SNe Ia around voids

In this section, we consider the repartition of the 281 ZTF SNe Ia within the SDSS footprint according to their distance from the centre of the nearest neighbouring voids, as obtained from the method detailed in Sect. 2.3.

We normalised the void-centric distance by the radius of the corresponding voids. This normalisation means that the subsequent analysis is independent of the different scales of the void sample. Figure 3 displays the corresponding distribution for the

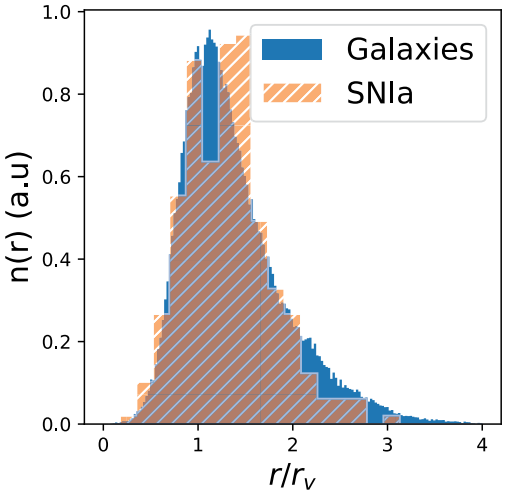

Fig. 3. Void-centric distance of galaxies and SNe Ia distribution.

SNe Ia and galaxies matched with the same procedure. The SNe Ia distribution covers a similar distance range to that of galaxies and follows a similar behaviour, that is, there are a small number of SNe Ia near the centre of the voids, with this number steadily increasing and reaching a maximum value before decreasing again at greater separation, $r/r_v > 2$. This suggests that SNe Ia also sample the large-scale structure, as galaxies do, as shown in Tsaprazi et al. (2022). However, we note that the galaxy sample underlying the SNe Ia distribution might not be the same as that probed by the SDSS sample. Most SNe Ia in this sample are found within the range of 1–2 R/R_v, which corresponds to the characteristic compensating wall region surrounding voids, and encapsulates the denser parts of the large-scale structure, such as clusters and filaments.

Figure 4 displays the scattered stretch (top main panel) and colour (bottom main panel) of each SN Ia according to its normalised distance from the centre of their nearest void. The dashed line shows the median in each bin to mitigate the effect of outlier values. Concerning the distribution of the stretch with respect to the distance to the void centre, the running median shows no significant trend for the stretch in the outer part of the void centre. The population of SNe Ia available below $0.8r/r_v$ decreases significantly, and it seems that the number of low-stretch (negative) SNe Ia in this range decreases as well. The inner part of the void centre $<0.5r/r_v$ seems to favour positive stretch, but we note that the number of SNe Ia in this region is 5. Regarding the colour, again, the running median shows no significant trend towards a favoured intrinsic colour regime within voids. It is interesting however to note that the number of outlier values significantly decreases in the innermost part from the void centre.

Selecting a significant void sample with radii of $\geq 10\,\mathrm{Mpc\,h^{-1}}$, we find no significant behaviour of the stretch or colour as a function of the void-centric distance of the SN Ia. While this lack of behaviour could be attributed to a non-dependency of the SN Ia intrinsic properties on the under-dense environment of the LSS, some additional factors might come into play. The void definition used in this paper does not impose a shape (e.g. sphericity), and therefore the void-finding process might include higher-density regions surrounding the voids in their definition. This probably results in a bias in the void centre definition and the radius.

A second aspect to take into account is the lack of statistics at low r/r_v. Voids are, by definition, regions where the quantity

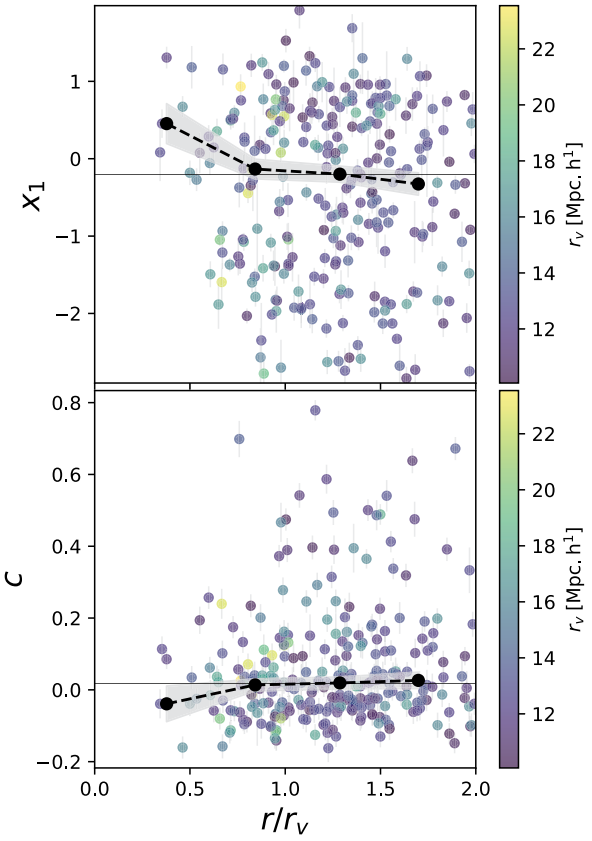

Fig. 4. Scatter plots of the intrinsic properties of SN Ia as a function of their distance from the void centre, normalised by the void radius. The upper panel displays the stretch x_1 and the lower panel displays the colour c of each SN Ia. The black dashed line with filled circle markers corresponds to the median value of the considered intrinsic property as a function of the centroidal (median) r/r_v in each bin. The shaded grey region represents the standard deviation normalised by the count in the bin. The horizontal line displays the median value of the considered intrinsic parameter in this sample. The marker colour indicates the void radius r_v in Mpc h^{-1} of the nearest neighbouring void to the SN Ia. There are 5, 76, 116, and 64 SNe Ia in the four uniform bins defined with the range $r/r_v = [0, 2]$.

of matter is lower than average. Thus, there are fewer galaxies inside voids and subsequently far fewer SNe Ia (Tsaprazi et al. 2022). One of the consequences is that the current SNe Ia sample might not allow us to sample the under-dense regions with high accuracy.

4. SNe Ia and Voronoi volume information

In this section, we consider the repartition of the ZTF SNe Ia properties within the SDSS footprint according to the Voronoi volume of their nearest neighbouring galaxy. As explained in Sect. 2.2, the void-finding process uses Voronoi tessellation to estimate the local density around each galaxy in order to proceed to the identification of low-density regions. The Voronoi volume is, by definition, indicative of the local density in the cosmic web: large (small) Voronoi volumes correspond to locally low(high)-density regions of the LSS.

Following from the section above, the void-centric distribution of the SN Ia intrinsic properties might be biased because the defined voids are not spherical and might encapsulate further selection effects, such as the inclusion of high-density galaxies in the ridge of the void, as mentioned in Sect. 2.2. The Voronoi

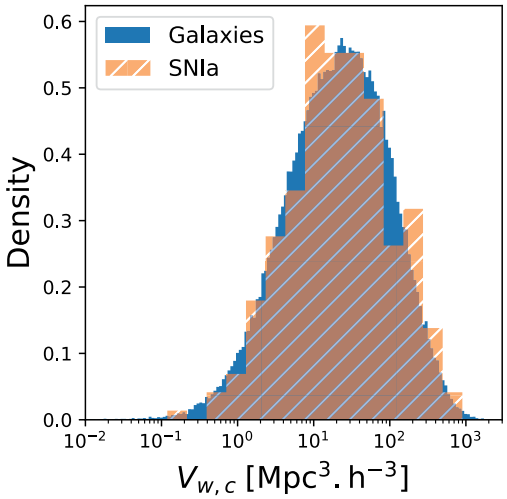

Fig. 5. Voronoi volume distributions of the galaxy sample and matched SNe Ia.

volume therefore allows us to have an additional local density estimate within the LSS, while avoiding potential systematic effects involved in the definition of voids. In addition, this analysis provides complementary information to that of Ruppin et al. (2025), who studied the ZTF SN Ia light-curve properties with respect to their proximity to clusters, as the Voronoi volumes enable us to probe both high-density and low-density regions.

We make use of the matching of each SN to its nearest neighbouring galaxy, which was performed to discard SNe Ia too close to the edges of the survey. Then, each SN is associated with the weighted Voronoi volume $V_{w,c}$ corresponding to its paired galaxy. We use the weighted volumes, which are corrected for completeness, and the galaxy selection function. This analysis choice allows us to alleviate the correlation between the average Voronoi volume at a given redshift and the redshift of the matched galaxy. This also prevents us from probing the redshift drifts of SNe Ia (Nicolas et al. 2021; Popovic et al. 2025) as we investigate the relation between Voronoi volumes and the intrinsic properties of the matched SNe. Figure 5 shows the distributions of the Voronoi volume of the galaxy sample and the resulting distribution matched to the SNe Ia. Similar to the void-centric distance, SNe Ia do not seem to favour a volume range different from that of the galaxies.

4.1. SN Ia properties according to Voronoi volumes

As in the previous section, we investigate a possible dependency of the intrinsic properties, namely the stretch x_1 and the colour c, on the weighted Voronoi volume of their matched galaxy. We define six bins of Voronoi volumes in Mpc^3 h^{-3} from the minimum Voronoi volume matched to a SN Ia to its maximum in order to map the different local densities across the range of available volumes, where the last (biggest) volume bin is considered to probe the most under-dense environment.

Figure 6 displays the scattered stretch (top main panel) and colour (bottom main panel) of each SN Ia according to the Voronoi volume of their nearest galaxy. The dashed line shows the median stretch in each bin to mitigate the effect of outlier values. In the stretch distribution with respect to the matched Voronoi volumes, a strong increase in the stretch can be seen as the volume grows until the median Voronoi volume of the galaxy sample, $\bar{V}_c^w = 21.80\,\mathrm{Mpc}^3\,\mathrm{h}^{-3}$, is reached (vertical dashed

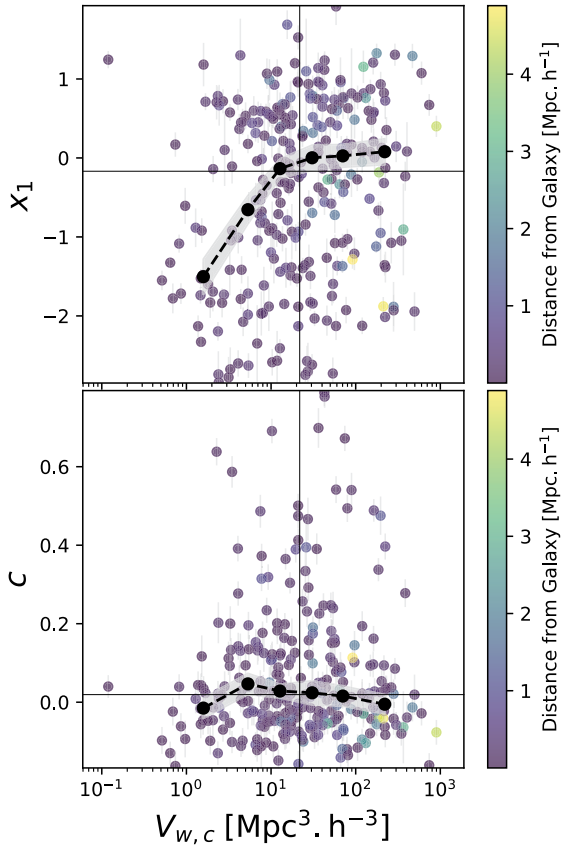

Fig. 6. Scatter plots of the intrinsic properties of SN Ia as a function of the Voronoi volume in Mpc^3 h^{-3} of the nearest galaxy to the SN Ia. The upper panel displays the stretch x_1 and the lower panel displays the colour c of each individual matched SN Ia. The black dashed line with filled circled markers corresponds to the median value of the considered intrinsic property in each bin of volume; the volume values are taken to be the centroidal median values in each bin. The shaded grey region represents the standard deviation normalised by the count in the bin. In ascending order of volume, there are 30, 40, 65, 57, 49, and 39 SNe Ia in the bins. Vertical lines represent the median weighted Voronoi volume of the galaxies, $\bar{V}_c^w = 21.80\,\mathrm{Mpc}^3\,\mathrm{h}^{-3}$, and horizontal lines represent the median value of the considered intrinsic parameter in the sample. The marker colour indicates the distance in Mpc h^{-1} from the nearest neighbouring galaxy to the SN Ia.

line). This trend is then suppressed after crossing into the sparser (less dense) region of Voronoi volume, which we define to be $V_c^w > \bar{V}_c^w$. A relation can therefore be drawn between SNe Ia with negative stretch and high-density regions of the LSS. In the case of the colour of the SNe, no dependency can be seen.

Following the observed trend, we separate the SN Ia stretch sample into two distinct subsamples: the over-dense subsample contains SNe Ia with a matched volume below the median value of the galaxy sample and the under-dense subsample contains SNe Ia with a matched volume above the median value of the galaxy sample. Figure 7 shows the resulting stretch distributions of the two selected samples, as well as that of the full SN Ia sample used in this analysis. The Kolmogorov–Smirnoff test applied to the two subsamples returns a p-value of 0.029, meaning that there is only a 2.9% probability that the samples originate from the same distribution. We can see that the low-stretch end is more populated in the over-dense bin than in the under-dense one compared to the complete sample distribution.

We can now attempt to understand exactly how the Voronoi volumes affect the stretch distribution. To do so, we suppose

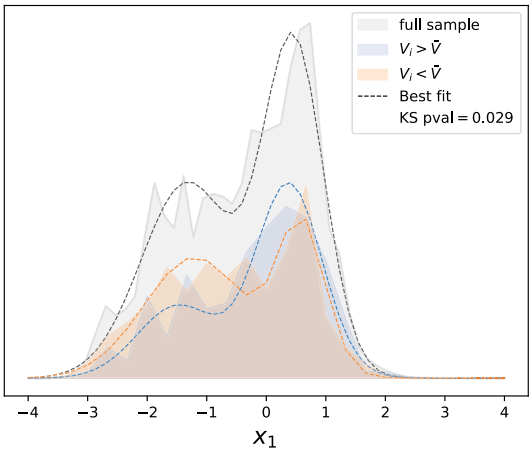

Fig. 7. Ideograms of the stretch in the full sample (shaded black), in the low-density environment sample (shaded blue), and in the high-density environment sample (shaded orange). The distributions are superimposed with their corresponding best-fitting bimodal stretch PDF (dashed lines) defined in Eq. (3) with corresponding parameters quoted in Table 2. The p-value for the Kolmogorov-Smirnoff test applied to the low- and high-density environment is provided in the legend and implies a significant difference.

that the probability distribution function (PDF) of the stretch distribution is bimodal (Rigault et al. 2020; Nicolas et al. 2021) and can be described as a simple mixture of two Gaussian distributions:

$$\mathcal{P}(x_1) = r\mathcal{N}\left(\mu_{x_1}^{\text{high}}, \tilde{\sigma}_{x_1}^{\text{high}}\right) + (1-r)\mathcal{N}\left(\mu_{x_1}^{\text{low}}, \tilde{\sigma}_{x_1}^{\text{low}}\right), \tag{3}$$

where $\mathcal{N}$ is a normal distribution, and is characterised by its mean stretch μ_{x_1} and standard deviation $\tilde{\sigma}_{x_1}$, and r is the fraction of SNe Ia belonging to the high-stretch mode. The $\tilde{\sigma}_{x_1}$ is defined as follows:

$$\tilde{\sigma}_{x_1}^{\text{high/low }2} = \sigma_{x_1}^{\text{high/low }2} + \Delta_{x_1}{}^2, \tag{4}$$

where Δ_{x_1} is the error of the measured stretch.

We fit this parametric model to the total sample and the subsamples by minimising the following log-likelihood:

$$\log \mathcal{L} = -2 \sum_i \log \mathcal{P}(x_1^i | \theta, \Delta x_1^i), \tag{5}$$

where $\mathcal{P}$ is defined in Eq. (3), wherein θ is the varied parameter vector and x_1^i and Δx_1^i are the stretch and error on the stretch provided by the SALT2.4 model. We performed the minimisation with the `iminuit` package (James & Roos 1975; Dembinski et al. 2020). The resulting best-fitting values to the model are quoted in Table 2. The best-fitting values to the full sample agree within 1σ with those fitted in Ginolin et al. (2024). When comparing the over-dense and under-dense cases quoted in the table, we can see that the parameter most affected by the split into two volume categories is the fraction of SNe Ia in the high-stretch mode r. We reach a 2.52σ significance of the difference of the best-fitting fractions between the Under-dense bin and the Over-dense bin. The best-fitting mean stretch values in the low and high modes differ with no and moderate significance of 0.86σ and 1.37σ, respectively. The best-fitting standard deviations of the high mode also reach a 1.41σ difference. An explanation for this is provided in Fig. 6, where we can see that the dense stretch distribution has a much more defined bimodal shape, with a sharp high-stretch mode. In the case of the under-dense bin, the transition between the two Gaussian mixtures appears smoother.

4.2. SN Ia repartition according to Voronoi volumes

Above, we consider all SNe Ia as being of the same type. We now consider a possible dependency of these subtypes on their local density environment, as probed by the Voronoi volumes. The resulting counts of SNe Ia according to the volumes of their matched galaxies and the repartition of subtypes are represented in Fig. 8. The subtypes are distributed into three broad categories: *cosmo*, *snia*, and *peculiar* (pec). The *cosmo* category encapsulates most norm or 91t SNe Ia, *snia* categorises SNe Ia that cannot be classified as norm with certainty, and the *peculiar* category accounts for non-norm or non-91t SNe Ia; further details on this classification process and analyses of SNe Ia subtypes can be found in the ZTF companion papers, Dimitriadis et al. (2025), Burgaz et al. (2025).

To perform this simple check, we opened up the selection of our data to all 448 SNe Ia found within the SDSS survey, as presented in Sect. 2.3. This is necessary as most of the SNe Ia subtyped as peculiar do not pass the quality cut applied to our analyses.

Figure 8 shows the fractions of the different types of SNe Ia in each of the volume bins, from the densest part of the sample to the sparsest, as well as the corresponding histogram counts of the SNe Ia according to their types (the first stacked histogram) and their matched volume (the second stacked histogram). The error bars are computed by considering the Poisson counts in each bin. About 79% of the SNe Ia are classified as *cosmo*, 7.6% as *peculiar,* and 13.4% as *snia*. The repartition of those subtypes in the different local environments is in general accordance with that of the total sample, within 1σ, except for the population of *peculiar* SN Ia in the densest bin $V_{w,c}^1$, accounting for 17% of the SNe Ia detected in this range, which is a 1.7σ difference from the SN Ia fraction computed over the totality of our sample. These *peculiar* SNe Ia in the densest bin are mostly *91bg* types. Considering these statistics, we can conclude that there is a very moderate dependency of SN Ia subtype on the local density environment. This moderate dependency is due to *peculiar* SNe Ia that appear to be more prevalent in over-dense environments. When considering the quality cuts applied to obtain a cosmological SNe Ia sample, this dependency disappears as most of the *peculiar* do not pass these cuts.

5. Discussion

Throughout this paper, we investigate the relationship between the large-scale environment of SN Ia and their properties, with a particular focus on voids and overall under-dense environments. We first considered the environment traced by voids identified in the SDSS-DR7 galaxy sample and then extended the analysis to using the Voronoi volumes of the galaxies – which are a by-product of the void-finding process – as a tracer of local density in the LSS.

Most SNe Ia are found at a distance of $r/r_v > 0.5$, which attests to their prevalence in medium- to high-density environments such as filaments, walls, and clusters. This observation also confirms that SNe Ia sample the galaxy density field, having a similar radial density, in accordance with Tsaprazi et al. (2022) clustering evidence. We observe 1.8% of SNe Ia in the selected sample to be found in highly under-dense environments with $r/r_v < 0.5$, while Tsaprazi et al. (2022), with a sample of 498 SNe Ia, found about 4% of those to be embedded

Table 2. Best-fitting parameters to the Gaussian mixture PDF of the stretch distribution.

Sample	Full	Over-dense	Under-dense
$\mu_{x_1}^{\rm low}$	-1.33 ± 0.20	-1.20 ± 0.20	-1.49 ± 0.25
$\sigma_{x_1}^{\rm low}$	0.75 ± 0.13	0.83 ± 0.14	0.65 ± 0.17
$\mu_{x_1}^{\rm high}$	0.46 ± 0.11	0.59 ± 0.11	0.38 ± 0.10
$\sigma_{x_1}^{\rm high}$	0.48 ± 0.07	0.36 ± 0.10	0.53 ± 0.07
r	0.53 ± 0.09	0.37 ± 0.09	0.68 ± 0.08

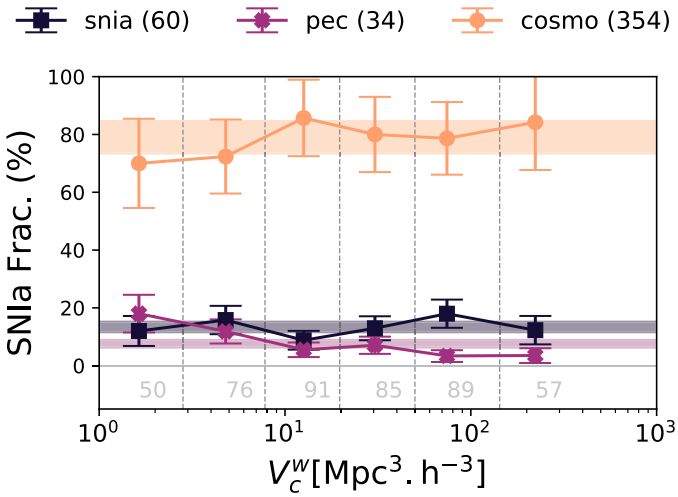

Fig. 8. SN Ia subtype fractions as a function of the binned nearest galaxy volumes in Mpc^3 h^{-3}. The shaded horizontal bands correspond to the fractional repartition of the SNe Ia subtypes in the total sample of 448 SNe Ia. In the inset legend, we quote the number of SNe Ia in each subtype category. The vertical dotted lines delineate the volume bins used to quote the percentage; we also quote in grey text the corresponding number of SNe Ia in each volume bin.

in voids detected in density field reconstruction. We therefore detect fewer SNe Ia near voids than these latter authors do, which can be attributed to the void definition procedure, ours being geometrical while theirs is dynamical. We still find consistent fractions between both galaxy and SN Ia samples in the under-dense part of the voids. Beyond the similar clustering behaviour of SNe Ia around voids, we detect no significant behaviour of the SN Ia properties with respect to the normalised void-centric distance of the SNe Ia. However, this lack of evidence cannot be solely attributed to a lack of colour, and especially stretch dependency in the void vicinity, given the additional effects that might come into play. Voids are, by definition, underpopulated environments, and so our analysis may be limited by the SN Ia statistics, especially in the range $[0-1]r/r_{\rm v}$ of the void centre, preventing the robust detection of any possible relation. A second statistical aspect might be the lack of void statistics, limited by the sky coverage of the source galaxy sample. Additionally, while some stringent cuts were applied to mitigate possible spurious voids, other systematic effects might be coming into play in the void definition, such as off-centring or over-estimation of the radii. The definition from the Voronoi volume provides local density information, and the defined voids might be part of an overall denser or more under-dense part of the Universe. Some of these effects might be averaged out in the statistical two-point analyses, but not with the methodology adopted in this paper.

When considering the local environment provided by the weighted Voronoi volumes, we find a strong dependency between stretch and density: the denser the environment, the lower the median stretch. This behaviour is in full agreement with the cluster-centric distribution of the stretch pointed out by Larison et al. (2024) and shown in the Ruppin et al. (2025) ZTF-DR2 companion paper. Using the Voronoi volumes, we can trace the full evolution from the highest-density regions of the sample to the lowest. The volumes, in comparison to the cluster matching in the Ruppin et al. (2025) analysis, enable us to categorise the SN Ia large-scale environment and access locally dense environments, such as dense galaxy groups or undetected clusters. Indeed, the Ruppin et al. (2025) study points out that the cluster sample is incomplete for masses $M_{500} \lesssim 10^{13}\,M_\odot$ at $z \leq 0.1$. Voronoi volumes thus provide complementary information for those environments that are less dense than those galaxy clusters. The influence of the LSS seems stronger in high-density environments than in low-density environments when considering the scattered distribution. There can be several reasons for this behaviour. Firstly, high-density regions, and therefore small volumes, are better sampled than large volumes (low-density regions) because they are inhabited by objects of greater luminosity. Secondly, volumes in the middle to high volume range can, inversely, be less well sampled, especially at high redshifts, where faint objects are not detected. By modelling our stretch distribution with a bimodal model, we find that the Voronoi volume affects the fraction of SNe Ia belonging to the high-stretch mode. The decrease in the fraction of SNe Ia populating the high-stretch mode in locally dense environments is in accordance with the model considered by Ruppin et al. (2025) in the vicinity of clusters.

To overcome the possible lack of statistics or systematic errors intervening in the spatial distribution of the SNe Ia light-curve properties around voids, we considered the same properties when matched to their specific local environment. In this case, we do not consider the proximity to the most isolated galaxies but probe the whole range of densities available through the use of Voronoi volumes to test the impact of local density on the SNe Ia properties. The two methods considered in the paper are therefore complementary, as the first, related to the distance from the centre of the void, is a more global approach and allows us, in principle, to be more sensitive to the largest isolated area of the survey. The first caveat of this method is that the zone deep into the void is more affected by statistical fluctuations; the second is that SNe Ia belonging to different dense structures (filaments, clusters, walls) become merged with increasing separation distances. The second method offers a local description regarding the isolation of the SNe Ia. Indeed, a large Voronoi cell, despite being of low-density, might not be located near the void centre. This local density information is thus lost when considering distance from the void centre measurements. This methodology therefore provides a complementary information.

Finally, this method separates the different LSS environments, from the least dense environment to the most dense by definition, enabling us to probe the continuous evolution of the SNe Ia light-curve properties as a function of local density.

Although the stretch behaviour seems to depend on its local density environment, one might (legitimately) question whether this apparent dependency is actually originating from the LSS, and not from host galaxy properties, which the Voronoi volume might be sensitive to. Among the known environmental dependencies of SNe Ia, we refer to the local colour and global mass as used in Ginolin et al. (2024), wherein the authors show that the stretch distribution can be affected in two different ways with respect to the environmental tracer. The local colour affects mostly the fraction of SNe Ia in the high-stretch mode, while the global mass shifts the average value of the stretch mode. In comparison, the apparent shift – 1σ for the low stretch mode and above 1σ for the high stretch mode – toward lower stretch values in the under-dense volume bin is in opposition to the behaviour highlighted in Ginolin et al. (2024). This observation appears to be an argument for discarding our density environment tracer as a direct proxy for the global mass of the host galaxies. However, we note that the behaviour of the best-fitting parameters might also be due to the smoother transition between the low- and high-stretch modes in the under-dense bin than in the over-dense bin, which displays a much stronger bimodality. Ruppin et al. (2025) discarded this hypothesis as well, considering a similar parametrisation of the stretch mean values to that of Ginolin et al. (2024). However, in both our analysis and that of Ruppin et al. (2025), the density environment affects mostly the fraction of SNe Ia in the high-stretch mode, and therefore has a similar effect to the local colour of the host galaxy. Works related to the study of galaxy properties with respect to their local environment have revealed evidence for a colour–density relation, that is, a relation between the colour of galaxies and the local environment of those galaxies within the LSS (Bamford et al. 2009; Kauffmann et al. 2004), with redder galaxies being found in denser environments and bluer galaxies in less dense environments. This relation is further supported as galaxies within voids are less massive, bluer, and favour younger stellar environments with high specific star formation rates (Rojas et al. 2004; Ricciardelli et al. 2014, 2017; Florez et al. 2021; Habouzit et al. 2020). The latter properties correspond to host galaxies of high-stretch-mode SNe (Rigault et al. 2020; Nicolas et al. 2021).

In light of these pieces of information, we can consider that the probable dependency on the local density environment is most likely linked to specific galaxy properties such as colour. Under-dense environments should favour high-stretch SNe Ia, which already represent the dominant part of the stretch distribution; this could explain why no significant effect can be seen when considering Voronoi volumes.

6. Conclusion

Using a selection of 281 SNe Ia from the ZTF-Cosmo-DR2 sample overlapping with the Main Sample footprint of the SDSS galaxy survey, we investigated the relationship between the SN Ia properties stretch and colour and the distance to the centre of the nearest neighbouring voids. We identified voids within the low-redshift $z < 0.1$ galaxy spectroscopic sample from the SDSS-DR7 data. Beyond confirming that SNe Ia sample the density field in a similar manner to the SDSS galaxy distribution, we find no significant behaviour of the stretch or colour distribution with respect to the distance from the centre of the void, which is possibly due to a lack of signal or additional effects, such as low SN Ia sampling in the vicinity of the void or void selection.

Using the Voronoi volumes of the nearest neighbouring galaxy to each SN, we probed the dependency of stretch and colour on the local density of the SNe Ia. We find that small volumes, which probe high-density regions, significantly favour low-stretch SNe Ia. Our results are consistent with the effect detected with respect to the cluster-centric stretch distribution, which favours low stretches in the vicinity of the cluster (Ruppin et al. 2025). Volumes are also complementary, as they allow us to be more sensitive to locally high-density regions, such as galaxy groups, which do not pass the detection threshold to be qualified as clusters. This dependency affects the fraction of low-stretch/high-stretch SNe in the sample and not their average distribution, similar to the host local colour, as shown by Ginolin et al. (2024). Previous works also showed a relationship between the colour of galaxies and their local density in the large-scale environment. We thus consider that the dependency of SNe Ia on the LSS might be mostly driven by the colour of their host galaxies. Increased coverage of the ZTF footprint by a low-redshift-galaxy catalogue coupled with an increased SNe Ia sample might allow us to investigate this aspect further.

Such a relation should not lead to strong biases in the analysis of the Hubble Diagram, provided that the treated SNe Ia sample is homogeneous and unbiased towards a specific large-scale environment. The relation might however be relevant when relying on reconstruction techniques of the density and velocity fields, considering that SN Ia distance moduli might be loosely dependent on the spatial repartition of SNe Ia in the LSS.

Acknowledgements. This work has been supported by the Agence Nationale de la Recherche of the French government through the program ANR-21-CE31-0016-03. This project has received funding from the European Research Council (ERC) under the European Union's Horizon 2020 research and innovation program (grant agreement n 759194 – USNAC). GD, UB and JHT are supported by the UB is supported by the H2020 European Research Council grant no. 758638. L.G. acknowledges financial support from AGAUR, CSIC, MCIN and AEI 10.13039/501100011033 under projects PID2020-115253GA-I00, PIE 20215AT016, CEX2020-001058-M, and 2021-SGR-01270. This work has been supported by the research project grant "Understanding the Dynamic Universe" funded by the Knut and Alice Wallenberg Foundation under Dnr KAW 2018.0067 and the *Vetenskapsrådet*, the Swedish Research Council, project 2020-03444. Y.-L.K. has received funding from the Science and Technology Facilities Council [grant number ST/V000713/1]. T.E.M.B. acknowledges financial support from the Spanish Ministerio de Ciencia e Innovación (MCIN), the Agencia Estatal de Investigación (AEI) 10.13039/501100011033, and the European Union Next Generation EU/PRTR funds under the 2021 Juan de la Cierva program FJC2021-047124-I and the PID2020-115253GA-I00 HOSTFLOWS project, from Centro Superior de Investigaciones Científicas (CSIC) under the PIE project 20215AT016, and the program Unidad de Excelencia María de Maeztu CEX2020-001058-M. Based on observations obtained with the Samuel Oschin Telescope 48-inch and the 60-inch Telescope at the Palomar Observatory as part of the Zwicky Transient Facility project. ZTF is supported by the National Science Foundation under Grant No. AST-2034437 and a collaboration including Caltech, IPAC, the Weizmann Institute of Science, the Oskar Klein Center at Stockholm University, the University of Maryland, Deutsches Elektronen-Synchrotron and Humboldt University, the TANGO Consortium of Taiwan, the University of Wisconsin at Milwaukee, Trinity College Dublin, Lawrence Livermore National Laboratories, and IN2P3, France. Operations are conducted by COO, IPAC, and UW. SED Machine is based upon work supported by the National Science Foundation under Grant No. 1106171. The ZTF forced-photometry service was funded under the Heising-Simons Foundation grant #12540303 (PI: Graham). The Gordon and Betty Moore Foundation, through both the Data-Driven Investigator Program and a dedicated grant, provided critical funding for SkyPortal. Funding for the Sloan Digital Sky Survey (SDSS) has been provided by the Alfred P. Sloan Foundation, the Participating Institutions, the National Aeronautics and Space Administration, the National Science Foundation, the U.S. Department of Energy, the Japanese Monbukagakusho, and the Max Planck Society. The SDSS Website is `http://www.sdss.org/`. The SDSS is managed by the Astrophysical Research Consortium (ARC) for the Participating Institutions. The Participating Institutions are The University

of Chicago, Fermilab, the Institute for Advanced Study, the Japan Participation Group, The Johns Hopkins University, Los Alamos National Laboratory, the Max-Planck-Institute for Astronomy (MPIA), the Max-Planck-Institute for Astrophysics (MPA), New Mexico State University, University of Pittsburgh, Princeton University, the United States Naval Observatory, and the University of Washington.

References

Abazajian, K. N., Adelman-McCarthy, J. K., Agüeros, M. A., et al. 2009, ApJS, 182, 543
Abbott, T. M. C., Acevedo, M., Aguena, A., et al. 2024, ApJ, accepted [arXiv:2401.02929]
Amenouche, M., Rosnet, P., Smith, M., et al. 2025, A&A, 694, A3 (ZTF DR2 SI)
Aubert, M., Cousinou, M.-C., Escoffier, S., et al. 2022, MNRAS, 513, 186
Bamford, S. P., Nichol, R. C., Baldry, I. K., et al. 2009, MNRAS, 393, 1324
Bellm, E. C., Kulkarni, S. R., Graham, M. J., et al. 2019, PASP, 131, 018002
Betoule, M., Kessler, R., Guy, J., et al. 2014, A&A, 568, A22
Blagorodnova, N., Neill, J. D., Walters, R., et al. 2018, PASP, 130, 035003
Blanton, M. R., Schlegel, D. J., Strauss, M. A., et al. 2005, AJ, 129, 2562
Bonici, M., Carbone, C., Davini, S., et al. 2023, A&A, 670, A47
Brout, D., Dan, S., Brodie, P., et al. 2022, ApJ, 938, 110
Burgaz, U., Maguire, K., Dimitriadis, G., et al. 2025, A&A, 694, A9 (ZTF DR2 SI)
Childress, M., Aldering, G., Antilogus, P., et al. 2013, ApJ, 770, 108
Childress, M. J., Wolf, C., & Zahid, H. J. 2014, MNRAS, 445, 1898
Contarini, S., Ronconi, T., Marulli, F., et al. 2019, MNRAS, 488, 3526
Contarini, S., Verza, G., Pisani, A., et al. 2022, A&A, 667, A162
Dekany, R., Smith, R. M., Riddle, R., et al. 2020, PASP, 132, 038001
Dembinski, H., Ongmongkolkul, P., Deil, C., et al. 2020, https://doi.org/10.5281/zenodo.3949207
Dimitriadis, G., Burgaz, U., Deckers, M., et al. 2025, A&A, 694, A10 (ZTF DR2 SI)
Filippenko, A. V. 1989, PASP, 101, 588
Florez, J., Berlind, A. A., Kannappan, S. J., et al. 2021, ApJ, 906, 97
Freedman, W. L. 2021, ApJ, 919, 16
Ginolin, M., Rigault, M., Smith, M., et al. 2024, A&A, submitted [arXiv:2405.20965] (ZTF DR2 SI)
Graham, M. J., Kulkarni, S. R., Bellm, E. C., et al. 2019, PASP, 131, 078001
Gregory, S. A., & Thompson, L. A. 1978, ApJ, 222, 784
Guy, J., Astier, P., Baumont, S., et al. 2007, A&A, 466, 11
Guy, J., Sullivan, M., Conley, A., et al. 2010, A&A, 523, A7
Habouzit, M., Pisani, A., Goulding, A., et al. 2020, MNRAS, 493, 899
Hamaus, N., Aubert, M., Pisani, A., et al. 2022, A&A, 658, A20
Hamilton, A. J. S., & Tegmark, M. 2004, MNRAS, 349, 115
Hamuy, M., Phillips, M. M., Schommer, R. A., et al. 1996, AJ, 112, 2391
Hoyle, F., & Fowler, W. A. 1960, ApJ, 132, 565 [Erratum: ApJ, 134,1028 (1961)]
Hoyle, F., Rojas, R. R., Vogeley, M. S., & Brinkmann, J. 2005, ApJ, 620, 618
James, F., & Roos, M. 1975, Comput. Phys. Commun., 10, 343
Jôeveer, M., Einasto, J., & Tago, E. 1978, MNRAS, 185, 357
Kauffmann, G., White, S. D. M., Heckman, T. M., et al. 2004, MNRAS, 353, 713
Kelly, P. L., Hicken, M., Burke, D. L., Mandel, K. S., & Kirshner, R. P. 2010, ApJ, 715, 743
Kelsey, L., Sullivan, M., Wiseman, P., et al. 2023, MNRAS, 519, 3046
Kenworthy, W. D., Jones, D. O., Dai, M., et al. 2021, ApJ, 923, 265
Kim, Y.-L., Smith, M., Sullivan, M., & Lee, Y.-W. 2018, ApJ, 854, 24
Kim, Y.-L., Kang, Y., & Lee, Y.-W. 2019, J. Korean Astron. Soc., 52, 181
Kim, Y. L., Rigault, M., Neill, J. D., et al. 2022, PASP, 134, 024505
Krause, E., Chang, T.-C., Doré, O., & Umetsu, K. 2013, ApJ, 762, L20
Lampeitl, H., Nichol, R. C., Seo, H. J., et al. 2010, MNRAS, 401, 2331
Larison, C., Jha, S. W., Kwok, L. A., & Camacho-Neves, Y. 2024, ApJ, 961, 185
Mao, Q., Berlind, A. A., Scherrer, R. J., et al. 2017, ApJ, 835, 161
Masci, F. J., Laher, R. R., Rusholme, B., et al. 2019, PASP, 131, 018003
Möller, A., Wiseman, P., Smith, M., et al. 2024, MNRAS, 533, 2073
Nadathur, S., Carter, P. M., Percival, W. J., Winther, H. A., & Bautista, J. E. 2019, Astrophysics Source Code Library [record ascl:1907.023]
Neyrinck, M. C. 2008, MNRAS, 386, 2101
Nicolas, N., Rigault, M., Copin, Y., et al. 2021, A&A, 649, A74
Padmanabhan, N., Schlegel, D. J., Finkbeiner, D. P., et al. 2008, ApJ, 674, 1217
Pan, D. C., Vogeley, M. S., Hoyle, F., Choi, Y.-Y., & Park, C. 2012, MNRAS, 421, 926
Pedregosa, F., Varoquaux, G., Gramfort, A., et al. 2011, J. Mach. Learn. Res., 12, 2825
Perlmutter, S., Aldering, G., Goldhaber, G., et al. 1999, ApJ, 517, 565
Phillips, M. M. 1993, ApJ, 413, L105
Pisani, A., Sutter, P. M., Hamaus, N., et al. 2015, Phys. Rev. D, 92, 083531
Pisani, A., Massara, E., Spergel, D. N., et al. 2019, BAAS, 51, 40
Popovic, B., Brout, D., Kessler, R., Scolnic, D., & Lu, L. 2021, ApJ, 913, 49
Popovic, B., Scolnic, D., Vincenzi, M., et al. 2024, MNRAS, 529, 2100
Popovic, B., Rigault, M., Smith, M., et al. 2025, A&A, 694, A5 (ZTF DR2 SI)
Pruzhinskaya, M., Novinskaya, A., Pauna, N., & Rosnet, P. 2020, MNRAS, 499, 5121
Radinović, S., Nadathur, S., Winther, H. A., et al. 2023, A&A, 677, A78
Ricciardelli, E., Cava, A., Varela, J., & Quilis, V. 2014, MNRAS, 445, 4045
Ricciardelli, E., Cava, A., Varela, J., & Tamone, A. 2017, ApJ, 846, L4
Riess, A. G., Press, W. H., & Kirshner, R. P. 1996, ApJ, 473, 88
Riess, A. G., Filippenko, A. V., Challis, P., et al. 1998, AJ, 116, 1009
Riess, A. G., Yuan, W., Macri, L. M., et al. 2022, ApJ, 934, L7
Rigault, M., Neill, J. D., Blagorodnova, N., et al. 2019, A&A, 627, A115
Rigault, M., Brinnel, V., Aldering, G., et al. 2020, A&A, 644, A176
Rigault, M., Smith, M., Goobar, A., et al. 2025, A&A, 694, A1 (ZTF DR2 SI)
Rojas, R. R., Vogeley, M. S., Hoyle, F., & Brinkmann, J. 2004, ApJ, 617, 50
Rubin, D., Aldering, G., Betoule, M., et al. 2023, ApJ, submitted [arXiv:2311.12098]
Ruppin, F., Rigault, M., Ginolin, M., et al. 2025, A&A, 694, A6 (ZTF DR2 SI)
Sánchez, C., Clampitt, J., Kovacs, A., et al. 2017, MNRAS, 465, 746
Sheth, R. K., & van de Weygaert, R. 2004, MNRAS, 350, 517
Smith, M., Rigault, M., et al. 2025, A&A, in prep. (ZTF DR2 SI)
Sullivan, M., Conley, A., Howell, D. A., et al. 2010, MNRAS, 406, 782
Sutter, P. M., Lavaux, G., Hamaus, N., et al. 2015, Astron. Comput., 9, 1
Swanson, M. E. C., Tegmark, M., Hamilton, A. J. S., & Hill, J. C. 2008, MNRAS, 387, 1391
Taylor, G., Jones, D. O., Popovic, B., et al. 2023, MNRAS, 520, 5209
Toy, M., Wiseman, P., Sullivan, M., et al. 2023, MNRAS, 526, 5292
Tripp, R. 1998, A&A, 331, 815
Tsaprazi, E., Jasche, J., Goobar, A., et al. 2022, MNRAS, 510, 366
Woodfinden, A., Nadathur, S., Percival, W. J., et al. 2022, MNRAS, 516, 4307
Xavier, H. S., Gupta, R. R., Sako, M., et al. 2013, MNRAS, 434, 1443
Zaidouni, F., Veyrat, D., Douglass, K.A., & BenZvi, S. 2024, ApJ, submitted [arXiv:2403.20008]